CO_2 REACTIVE TRANSPORT IN LIMESTONE: FLOW REGIMES, FLUID FLOW AND MECHANICAL ROCK PROPERTIES

H. Ott,[a,1,2] S. Oedai,[1] C. H. Pentland,[1] K. Eide-Engdahl,[1] A. J. van der Linden,[1] O. Gharbi,[1,2] A. Bauer[1] and A. Makurat[1]

(1) Shell Global Solutions International B.V., The Netherlands.
(2) Imperial College London, Department of Earth Science & Engineering, United Kingdom.

This paper was prepared for presentation at the International Symposium of the Society of Core Analysts held in Napa Valley, California, USA, 16–19 September 2013

ABSTRACT

The influence of chemical reactions between injected CO_2, formation fluids and the target rock formation leads to uncertainties for geological sequestration projects. Reactions may influence the fluid-flow field, i.e. reactive transport, and the mechanical rock properties, which might degrade, leading to uncertainties with respect to the rock integrity in the affected region. We investigate both the influence of calcite dissolution on the fluid flow and the mechanical rock properties for two cases: first under realistic CO_2/brine field flow rates leading to heterogeneous dissolution, i.e. wormholing, and second under no-flow conditions leading to a rather homogeneous dissolution. We find a significant influence of dissolution on single- and two-phase flow and changes of the elastic rock properties and the failure behavior. The study is an essential step toward understanding CO_2 plume migration and the effects caused by long-term migration of CO_2 in carbonate reservoirs, providing input parameters for reservoir models and reservoir surveillance.

INTRODUCTION

From work on well stimulation, we know that the injection of acids in carbonate rocks can lead to the formation of highly conductive flow channels, i.e. wormholes (WH) [1–3]. These channels significantly enhance the flow of reservoir fluids, since conductivity in WH is usually orders of magnitude higher than of the unaltered or surrounding rock matrix. Therefore, matrix acidizing often successfully improves well productivity when the formation around the well bore is tight or damaged [1–3]. It is likely that WHs or – more generally – heterogeneous dissolution patterns are caused by CO_2 injection in water-bearing carbonate fields or aquifers [4,5]. In those cases, the situation is slightly more complex than for matrix acidizing. The acid is not injected, but forms in the rock under two-phase flow conditions at the same time as reactions with the rock matrix occur. Significantly greater quantities of CO_2 are typically injected for sequestration than acid for well stimulation purposes – up to hundreds of cubic meters for acid stimulation [3] to millions of cubic meters liquid CO_2 for industrial-scale CCS projects [6]. The injected CO_2 phase is immiscible with the formation brine, lowering the mobility of the aqueous

phase. This leads to a saturation-dependent (volumetric phase saturation) flow velocity of the aqueous phase and hence to saturation-dependent Péclet (*Pe*) and Damköhler (*Da*) numbers. For single phase acid injection, *Pe* and *Da* numbers are known to determine the exact dissolution pattern [7,8].

In contrast to well stimulation operations, the formation of highly conducting channels are rather a concern for CO_2 injection, since a highly directional (channelized) flow of injected fluids leads to bypassing of rock matrix and hence to a poor utilization of the pore space for CO_2 storage. This also affects the contact (surface area) between CO_2 and formation brine and hence the dissolution of CO_2. Furthermore, the dissolution pattern cannot be designed as for matrix acidizing, where fluids are injected under optimized conditions. The dissolution pattern resulting from CO_2 injection is a given. It could therefore be unfavorable with respect to fluid flow and mechanical rock properties.

The field-related questions – where, when and which dissolution pattern may occur – are not straightforward to answer. They require knowledge of flow regimes as a function of time and space, information that is normally extracted from reservoir modeling. However, these flow regimes in turn depend on the change of the fluid-flow field and hence on the resulting dissolution patterns. Including this feedback mechanism in numerical modeling requires experimental data on structure formation and on fluid flow in the respectively modified rock structure.

The study presented here is an attempt to address these CO_2-specific issues of carbonate dissolution. We investigate the formation of dissolution patterns under single- and two-phase flow conditions and the influence of pattern formation on fluid flow. Furthermore, we address changes of mechanical rock properties for different dissolution mechanisms. The experiments discussed in this paper are listed in Table 1.

Experiments	Rock type ∅ x *L* [cm]	ϕ, *K* [mD]	*P*/*T* [bar/°C]	*Pe*/*Da*	Comments
Flooding sequences in Fig. 1	Estaillades limestone (7.5 x 15)	0.278, 270	100/50	$\sim 330^{b}/Y^{*}$	Figs. 1–5
WH formation in Fig. 6 Single-phase vs. two-phase flow	Euville limestone (2.54 x 10)	0.16–0.17, 270–360	100/50	$\sim 3000^{b}/\sim 0.1 \cdot Y$	Fig. 6
Mechanical rock properties	Euville limestone (3.8 x 7.6)	0.15–0.195, $80{,}450^{\dagger}$ 190–320‡	$100/50^{\dagger}$ 100/80‡	$\sim 150^{b}/\sim 2.2 \cdot Y^{\dagger}$ $\rightarrow 0^{b}/\rightarrow \infty^{\ddagger}$	Figs. 7, 8

Table 1: This is a summary of samples' properties and experimental conditions of the experiments presented in this paper. † Denotes data from WH and ‡ from RA experiments. * We give the *Da* number relative to the first experiment and assume the same specific reactive surface area for both rock types.

FLUID DISPLACEMENT IN THE UNALTERED ROCK

To study the influence of calcite dissolution on fluid flow we perform non-reactive single- and two-phase flow experiments in order to characterize the flow properties in unaltered rock, followed by a reactive flow experiment to modify the rock structure according to the intended flow regime. Subsequently, we repeat the initial non-reactive

experiments to test the influence of dissolution on fluid flow. A typical experimental sequence is shown in Fig. 1; the experiments **a** to **e** were carried out in a sequence on the same rock sample (Estaillades limestone), with cleaning steps between **b** and **c** and between **d** and **e**. We performed all experiments at 100 bar and 50°C, corresponding to an aquifer at a depth of about 1000 m. We follow the displacement processes by means of medical computer tomography (CT).

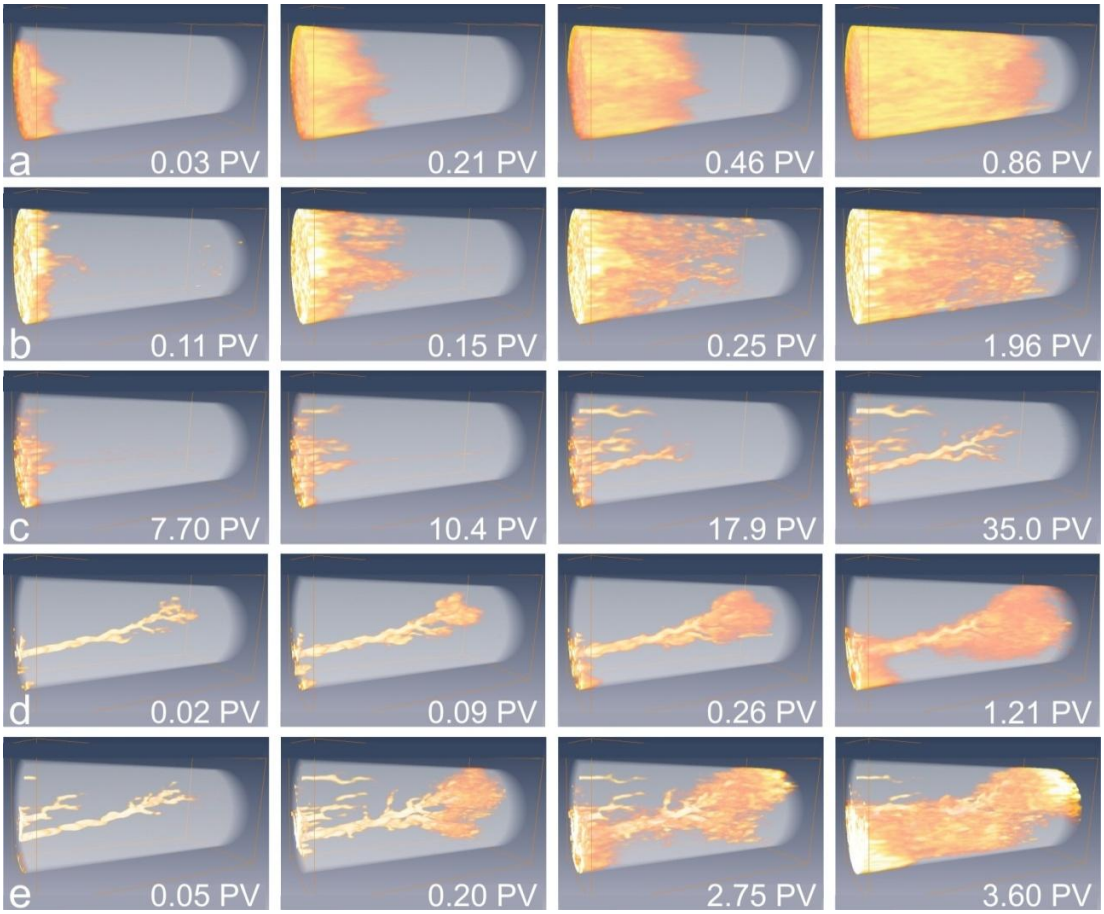

Figure 1: CT difference images of a series of core flood experiments in an Estaillades limestone sample. Visualized in orange: aqueous tracer concentration in a single phase flow experiment (experiments **a** and **d**), SC–CO_2 saturation in the primary drainage experiments **b** and **e**, and dissolved rock matrix in a reactive transport experiment, **c**. **a** and **b** were performed before the reactive experiment **c**, experiments **d** and **e** after **c**.

The top row, **a**, represents a time series of a tracer experiment. CsCl-doped brine was injected into a core pre-saturated with un-doped brine at a rate of 1 ml/min. Prior to flooding, the injected brine phase was equilibrated with CO_2 and the rock's mineralogy under experimental conditions in order to make the brine chemically and physically compatible with subsequent experimental steps. The tracer concentration was recorded by CT scanning and is displayed in orange in Fig. 1a, while the initial rock-fluid system is shown as a semi-transparent background. The images show the tracer front propagating nearly piston-like through the core as a function of injected fluid volume in units of the

total pore volume (PV). The flood front is slightly corrugated due to the intrinsic permeability variation of the rock sample. The tracer concentration at different time steps as a function of distance (moving from left to right) is shown in the left panel of Fig. 2 (blue lines). The slope of the concentration profile is changing with time, indicating the dispersion mainly because of the rock's heterogeneity. The tracer concentration reaches a value close to unity, showing a nearly complete miscible displacement without bypassing.

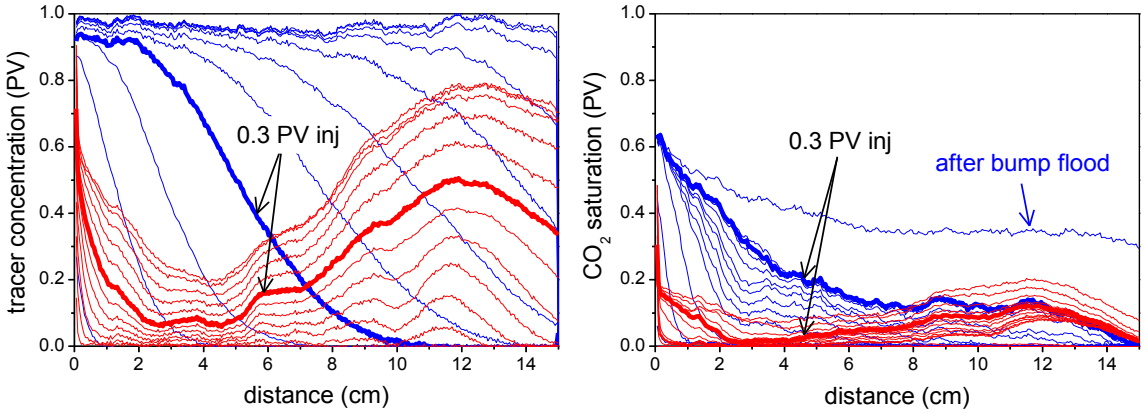

Figure 2: Saturation propagation during the experiments **a**, **b**, **d** and **e** in Fig. 1. Left: tracer concentrations during single-phase tracer tests of the unaltered sample (**a** – blue lines) and after WH formation (**d** – red line). The results of the CO_2-brine primary drainage experiments are shown in the right panel with the same color coding for the untreated (**b**) and treated (**e**) sample.

Subsequently, we injected CO_2 at a rate of 0.44 ml/min, immiscibly displacing the brine in the rock under experimental conditions in which CO_2 is in the supercritical (SC) state. The injected CO_2 was equilibrated with water prior to injection in order to avoid water dissolution during brine displacement. CO_2 dissolution into the brine phase and chemical rock-fluid interaction were suppressed by the fluid-fluid-rock equilibration as described above in step **a**. Fig. 1b shows the CT difference images during displacement at different time steps (in PV), in which orange represents the CO_2 saturation, while the initial rock-fluid system is shown as a semi-transparent background. While the single-phase tracer flow is sensitive to the heterogeneity of the permeability field, CO_2 primary drainage reacts on local variations of the capillary pressure and hence gives information about the p_C heterogeneity of the rock-fluid system [9,10]. Such unsteady-state experiments are used to determine the pair of relative permeability and capillary-pressure saturation functions, $k_r(S_W)$ and $p_C(S_W)$, in primary drainage (data not shown) [9]. The respective saturation profiles along the flow direction at different time steps are shown in the right panel of Fig. 2 (blue lines). The figure shows the propagation of the flood front through the core, leading to a relatively low average CO_2 saturation of about 0.2 after the breakthrough of CO_2. The higher CO_2 saturation at the inlet is attributed to the measured porosity profile and the respectively lower p_C at the inlet of the core. The brine production curve is shown in the left panel of Fig. 3. The low volume of brine produced during the experiment is a result of the low efficiency of brine displacement by CO_2 in the multi-porosity carbonate rock.

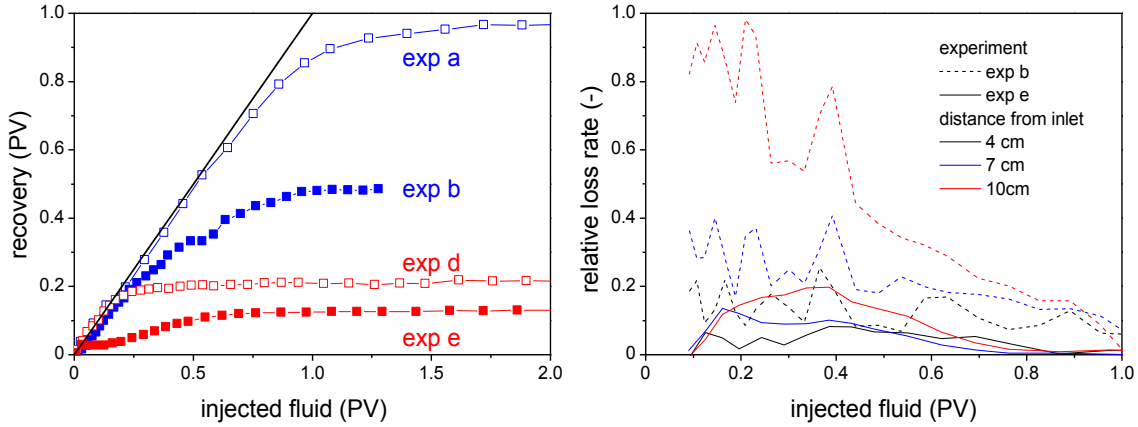

Figure 3: Left panel: brine production curves of the experiments **a**, **b**, **d** and **e** shown in Fig. 1. Right panel: fluid leak-off rates during experiments **b** and **e** at three positions from the inlet as indicated in the legend, representing the single WH and the ramified structure.

REACTIVE TRANSPORT: PATTERN FORMATION

We performed a number of reactive transport experiments in the course of the present study, following a similar experimental sequence to that presented in Fig 1. We find for different rock types (all limestone) and for different flow regimes that dissolution reactions generally increase intrinsic rock heterogeneity. Fig.1c shows an extreme case where WHs formed at relatively high *Pe* and *Da* numbers. We injected CO_2-saturated brine at a rate of ~1 ml/min into an initially brine-saturated core, leading to *Pe*=330.[b] In contrast to the core floods described above, the injected fluid was initially not equilibrated with the rock matrix, and hence rock dissolution occurs during the experiment. Fig. 1c shows the dissolved rock matrix as a function of injected fluid volume or as a function of time. Fluids as well as the initial rock are displayed semi-transparently while the dissolved rock volume is visualized in orange.

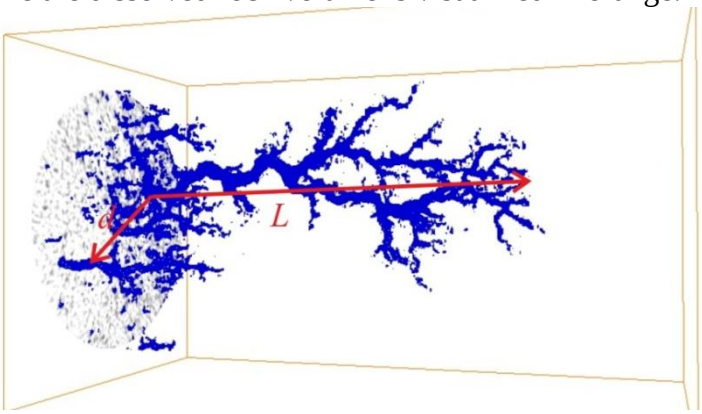

Figure 4: Detailed view of the dissolution pattern as shown in Fig. 1c. *L* represents the penetration depth of the WH and *d* the distance between two WHs.

Initially there are several “seed holes” formed, growing into the rock sample and reaching a certain length until they start competing with each other. Finally, one WH dominates

and starts forming branches. We stopped the experiment as the WH reached about 80% of the length of the sample.

Fluid conduction depends on the exact geometry of the dissolution pattern and the resulting flow controlling parameters. Fig. 4 shows the detailed structure of the WH; it shows a ramified and complex structure. Daccord and Lenormand for the first time described such dissolution pattern in terms of fractals [11] – i.e. self-similar geometric patterns. A fractal system is characterized by its dimension, α, which describes the fractal length of a WH l by $l=L^{\alpha}$, with L being the shortest length, i.e. the penetration depth of the WH. For the present case, we derive α~1.89. This value is higher than, but comparable to, values of ~1.6 derived for plaster of Paris systems studied by Daccord et al.

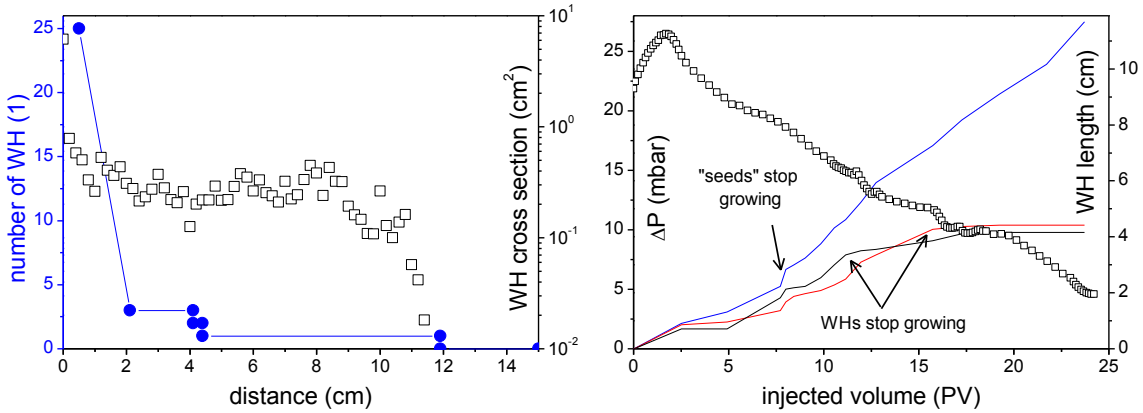

Figure 5: Left: static data obtained from the WH structure in Fig. 4: the number of WHs as a function of distance from the inlet (blue) and the total cross-section of the dissolution pattern in flow direction. Right: dynamic data of WH formation as shown in Fig. 1c; the pressure drop during experiment **c** and the length of the three most mature wormholes as a function of injected fluid volume.

The fractal dimension is a measure of branching. The question is whether the branching, respectively the *Pe* and *Da* numbers, influences the growth rate of the WH and to what extent it influences fluid conduction in single- and two-phase flow. Both questions relate to the total hydraulic cross-sections of the etched structure and the cross-sections of the individual WHs. The left panel of Fig. 5 shows the total hydraulic cross-section and the respective number of WHs as a function of distance from the sample inlet. Independent of the strong variation of the actual number of WHs and branches, the total hydraulic cross-section is rather constant apart from the "seed layer" at the inlet of the sample. Its value is in the order of 10^{-1} cm^2, which is large compared to the rock's permeability, which is in the order of 10^{-10} cm^2, leading to the observed high conductivity and to the bypassing of the rock matrix.

On a larger scale, the WH density will determine flow properties. For well stimulation, the density is often pre-defined by the well perforation. However, there might be an intrinsic length scale making up the density of WHs if there is no constraint. It is assumed that the WH density is determined by the competition for injected fluid. The largest WH shows typically the largest diameter and the most favorable pressure field, resulting in a

more rapid growth at the expense of shorter WHs that eventually stop growing [12,13]. Numerical simulations show that WHs interact with each other, i.e. reducing each other's flow rate. It was suggested that WHs compete when the distance between neighboring WHs (d) comes in the order of, or is less than, the length of the WHs (L), i.e. L/d~1 [12,14]. Even with the large sample size (3 inch ∅ in the present case), the cross-sectional area is too small to accommodate enough WHs to be representative and therefore there is just limited access to the WH density. However, the data in the right panel of Fig. 5 show this competition. Ignoring the branching, there are three dominant WHs at a time, corresponding to eight PVs with a similar length from which only one is growing further and the others stop growing. The ratio L/d to the longest WH is 0.9 and 1.7 for the second and third longest WH, respectively. This result is in line with the statements of Hoefner and Fogler (1988) and Buijse (1997) about WH competition [12,14].

CO_2-BRINE DISPLACEMENT IN THE ETCHED STRUCTURE

After the WH had formed, we repeated the initial flooding sequence – the single-phase tracer test and the subsequent injection of SC CO_2. Figs. 1d and 1e show the floods after WH formation and both are directly comparable to the initial floods in Figs. 1a and 1b, respectively. In both cases, the injected fluid mainly flows through the WH, bypassing the remaining rock matrix and spreading in the highly ramified "crown" and through the "tip" of the WH, leading to fluid displacement in radial and downstream directions, respectively. We attribute the radial displacement to fluid "loss", widening the WH system rather than increasing its length. This leakage rate into the surrounding matrix affects the acid transport to the actual tip of the WH and therefore has a strong influence on the growth rate, the maximum length and the structure of the WH [1].

A comparison of the longitudinal saturation profiles in Fig. 2 and the 3D images in Figs. 1d and 1e reveals some interesting features: the radial loss is strong at positions of high ramification ("the crown") and high WH density (at the inlet). In these regions the high number of holes and the small distances between individual holes allow for an effective fluid distribution in radial direction. The loss is less pronounced at the position of a single WH (between about 2 and 6 cm from the inlet).

The left panel of Fig. 3 shows the brine production curves associated with the saturation profiles and compares them to the production curves obtained from the floods of the unaltered rock **a** and **b**. In both cases, the displaced brine volume falls behind the production in the undisturbed experiments. The derivative of the tracer concentration and the CO_2 saturation, i.e. the rate of loss, for experiment **d** and **e** at three different positions is shown in the right panel of Fig 3. The positions measured from the inlet face were chosen to represent the fluid loss of the single WH (4 cm), the fully ramified "crown" (10 cm) and a position in between (7 cm). For single-phase flow (exp **d**), we expect a constant rate of loss, since brine-brine displacement at constant flow rate corresponds to a steady-state displacement. This is observed at the position of the single WH. The loss rate at the position of the crown is initially high, but is strongly declining in time. This is because the tracer distributes efficiently through the ramified structure but the integrated tracer concentration reaches a saturation value due to the finite cross-sectional area over

which we integrate. The true fluid loss rate is the initially high rate at the beginning of the flood. The CO_2-loss during the drainage experiment (exp **e**) is generally lower than the brine loss in exp **d**. It shows generally and especially at the position of the crown, a rate that starts from zero going through a maximum and then back to zero again. The occurrence of the maximum can be understood in terms of differential pressure. The CO_2 can just penetrate the matrix after overcoming the entry pressure, before which the rate of loss is zero. After penetrating the matrix, the respective differential pressure increases with penetration depth at a constant rate of loss, which slows down the rate. This effect will limit the radial loss of CO_2 and brine in a drainage situation. An interesting observation is that at positions of high ramification we reach a higher average CO_2 saturation than in the undisturbed matrix, while at positions of a single WH, the CO_2 saturation falls much behind the undisturbed case. In other words, the degree of ramification is a key parameter controlling bypassing due to wormholing.
However, the radial loss seems not to widen the individual channels, but rather to increase the ramification. This indicates that the fluids flow through the tips of the individual branches, rather than through their side walls. Our conclusion is that the fluid loss is mainly determined by the degree of ramification and eventually by the fractal dimension of the WH structure, i.e. linked to the *Pe* and *Da* numbers.

SINGLE-PHASE VS. TWO-PHASE REACTIVE TRANSPORT

For geological sequestration of CO_2, we envisage reactive transport to occur in single-phase flow (e.g. gravity-driven brine convection) and in two-phase flow (e.g. during the primary displacement process). The question therefore arises as to whether the simultaneous flow of an aqueous and a CO_2 phase suppresses wormholing, since the non-wetting phase will predominantly enter the low p_C regions of the rock matrix, which are essentially the WHs. If CO_2 enters as in Fig. 1e, the WH might not grow further, since the reactions take place between the rock's surface and the aqueous phase and not with the CO_2 phase. Following this idea, the presence of CO_2 should lead to a compact dissolution rather than to wormholing. We tested this idea in different core flood experiments, injecting CO_2-saturated brine (**f**), co-injecting CO_2 and brine into initially brine-saturated rock (**g**) and co-injecting CO_2 and brine into an initially CO_2-saturated rock sample (**h**). We performed this study on Euville limestone with CO_2 and brine injection rates of 1 ml/min at a 1″ diameter inlet face. The resulting $Pe \sim 3000$[b] is an order of magnitude higher than in the experiment shown above. In order to keep the global *Pe* number constant, the brine flow rate was kept the same in all three experiments.

Figure 6: WH formation under different conditions in single- and CO_2-brine two-phase flow. **f** WH after injection of CO_2-saturated brine, **g** after co-injection of CO_2 and brine in a brine-saturated rock sample (S_W=1), and **h** CO_2-brine co-injection into an initially CO_2-saturated sample (S_W=0). The experiments were performed at otherwise the same conditions and with the same brine injection rate, resulting in the same global *Pe* number for all experiments.

Fig. 6 shows the resulting dissolution patterns. The left image shows the result of the CO_2-saturated brine flood. As expected and in line with the observations in Fig. 1, a WH formed. We performed the second experiment in exactly the same way, but additionally co-injecting CO_2 at the same rate of 1 ml/min. Again, we observe WH formation. The WHs take individual pathways, but show a qualitatively similar structure.

As we have shown above, the displacement efficiency of CO_2/brine primary drainage is low. The resulting CO_2 saturation might even at a high CO_2 fractional flow be too small to prevent wormholing. In a third experiment (**h**), we attempted to increase the CO_2 saturation artificially by starting at 100% CO_2 saturation. Even in this case, we observe a similar dissolution pattern as in the previous cases **f** and **g**. These experiments indicate that the global *Pe* and *Da* numbers might determine the dissolution regime and that the presence of a second (non-wetting) fluid phase is of minor influence, which, however, needs further investigation.

MECHANICAL ROCK PROPERTIES

Mechanical rock properties such as stiffness and strength vary with the natural variation of porosity [15]. Since rock dissolution generally enhances porosity, we expect that those parameters will be affected by CO_2 injection as has been shown before [16]. This implies consequences for formation stability near the well bore and in the far field. In order to predict pore collapse and subsidence for the individual rock type and flow regime, we performed reactive experiments as discussed above, but in a triaxial compaction cell with in-situ monitoring of mechanical rock properties such as elasticity, acoustic velocities and point of failure.

While wormholing occurs in dynamic situations, we expect homogeneous dissolution to occur over longer time scales in the far field, either under “no-flow conditions” or close to chemical equilibrium. Homogeneous dissolution might lead to a stronger change of the mechanical rock properties and therefore we focus in the following on the comparison of both extreme dissolution regimes, following a study by IFP for the homogeneous dissolution [16,17].

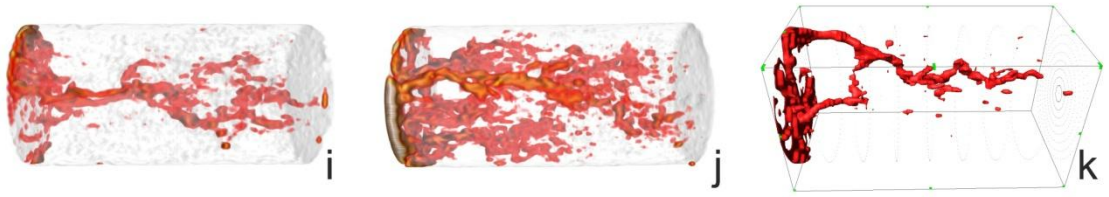

Figure 7: CT difference images of dissolution patterns in Euville limestone that have been formed after 3 (**i**) and 6 (**j**) retarded acid treatments and during injection of CO_2-saturated brine (**k**). Note that the CT contrast of **i** and **j** is strongly enhanced compared to the contrast of image **k**. The initial rock-fluid system is displayed as a semi-transparent background.

Due to the generally high reaction rate of carbonic acid with calcite, it is difficult to reach a homogeneous dissolution by means of CO_2 injection on a laboratory time scale, since the acid reacts already with the carbonates at the inlet face of the sample. For that reason, we used a retarded acid (RA) approach as developed in IFP to reach a more homogeneous dissolution pattern [17]. The RA aqueous solution we used is inactive at ambient temperatures and therefore does not react with the rock. Once injected into the core, the acid is activated under no-flow conditions by increasing the temperature, forming formic acid. The activated acid then dissolves the rock matrix until the solution is buffered. The buffered solution is subsequently removed by water injection. To continue dissolution, we repeat the treatment and we assume the dissolved rock volume to be proportional to the number of retarded acid treatments (RATs). Fig. 7 shows the dissolution patterns after three (**i**) and six (**j**) RATs. Image 7i suggests that channels are forming due to the treatment similar to the WH formation discussed before. However, in case of the RAT, the contrast of the CT images is strongly enhanced compared to image 7k in order to visualize the dissolution structure. The cause of the weak channels that have been formed during the RATs is probably related to the easier access of the RA solution in the high-permeability pathways where leaching takes place more efficiently by giving the inactive solution only a finite time for diffusion. We observe strong differences in the flow patterns (data not shown here) and in the rock mechanical parameters (discussed in the following), showing that the RA procedure was successfully applied. The results are directly compared to results of experiments on twin samples in which we inject CO_2-saturated brine at Pe~150,[b] i.e. Pe>>1, leading to WH formation as shown in Fig. 7k.

Fig. 8 presents data obtained for both dissolution regimes [18]. The left panel shows the normalized Young's modulus as a function of porosity change, reflecting the change of the rock's elastic properties. Interestingly, we observe only a minor impact of dissolution on the mechanical stiffness during wormhole formation. In contrast to this, the experiments showing a more homogeneous dissolution pattern as achieved by RATs exhibit a strong linear decay of elasticity. Despite the data scatter of the individual experiments, Young's modulus follows a clear trend and shows a qualitatively different behavior than in the experiments leading to WHs.

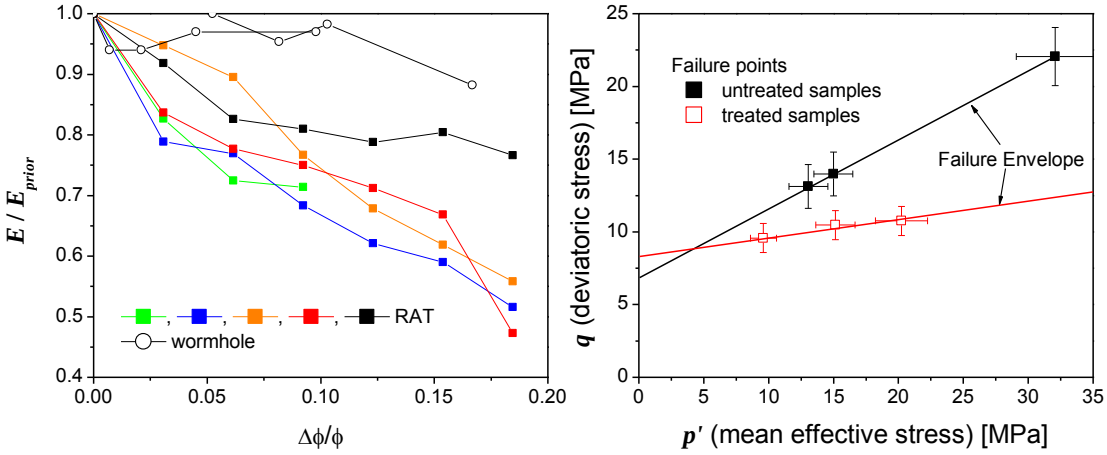

Figure 8: Left: Young's modulus as a function of porosity change for both heterogeneous (wormholing due to CO_2-saturated brine injection) and homogeneous (RAT) dissolution patterns. Right: Failure envelope of samples treated with RA and untreated samples (reference data).

Young's modulus and acoustic velocities (not shown) decrease more strongly than predicted by a natural porosity trend [18]. This indicates the local nature of the wormholing, which does not affect the rock matrix away from the WH. In contrast, the homogenous dissolution is likely to affect the grain-grain contacts and hence the mechanical rock properties.

In addition, the RATs might affect the rock strength. We performed failure tests of treated (after 6 treatments) and unaltered (reference) samples. The right panel of Fig. 8 shows the respective Mohr–Coulomb failure lines. The failure envelope of the treated samples falls below that of the reference samples, suggesting that homogeneous dissolution weakens the rock. The data shows a significant decrease in the friction angle. The change in the cohesion (ordinate axis intercept) is within the error bars and hence not significant.

SUMMARY AND CONCLUSIONS

We investigated reactive transport of CO_2 in limestone and the consequences of calcite dissolution for single-phase (brine-brine) and two-phase flow (CO_2-brine displacement). This study is work in progress, with the ultimate target of implementing structure formation during carbonate dissolution in continuum models for prediction of CO_2 storage. We focused on the CO_2-specific issues, in particular on two-phase flow, which is novel to this research area. Another area that is not yet well explored but is touched on in this paper is the influence of calcite dissolution on mechanical rock properties. We presented the change of stiffness and failure behavior for different dissolution regimes.

Key findings that we want to highlight are: (1) single- and two-phase reactive flow results in similar dissolution pattern for the same *Pe* number (same water injection rate at high *Pe*). (2) We observe complex WH structures with a high degree of ramification but with a roughly constant total cross-section, independent of the branching. We experimentally observed competition of WHs that is in reasonable agreement with findings out of earlier

numerical simulations. (3) We observe fluid loss with rates increasing with the degree of ramification. We find that at "typical" field flow rates, the loss leads rather to an increase of ramification than to a widening of individual channels. There is a less pronounced leak-off during CO_2 drainage than for miscible brine displacement. This might be a result of the differential pressure, which would build up during penetration into the rock matrix, resulting in a build-up of resistance against leak-off. (4) We find that localized dissolution, i.e. wormholing, has only limited influence on the mechanical rock properties. However, homogeneous dissolution substantially diminished rock elasticity and strength.

REFERENCES

a. Corresponding author; e-mail address: Holger Ott; holger.ott@shell.com, research@holger-ott.de.

b. We report global *Pe* and *Da* numbers referring to experimental geometries and injection rates. Often, local numbers are reported, describing reactions and transport in individual flow channels, i.e. on a microscopic scale.

1. A. D. Hill, R. S. Schechter and C. N. Fredd, in Economides and Nolte, Reservoir Stimulation, Schlumberger, third edition, 2001.
2. C. N. Fredd, in Economides and Nolte, Reservoir Stimulation, Schlumberger, third edition, 2001.
3. J. A. Robert and C. W. Crowe, in Economides and Nolte, Reservoir Stimulation, Schlumberger, third edition, 2001.
4. R. K. Svec and R. B. Grigg, SPE 71496, 1 (2001).
5. O. Izgec, B. Demiral, H. Bertin and S. Akin, *Transp. Porous Media* (2008) **72**, 1.
6. *IPCC Special Report on Carbon Dioxide Capture and Storage*, Cambridge University Press, UK, 2005.
7. G. Daccord, R. Lenormand and O. Lietard, *Chem. Eng. Sci.* (1993) **48**, 1, 169–178.
8. C. N. Fredd, and H. S. Fogler, *SPE Journal* (1999) **4**, 3, 196–205.
9. S. Berg, S. Oedai, and H. Ott, *Int. J. Greenhouse Gas Control* (2013) **12**, 478–492.
10. R. Pini, S. C. M. Krevor and S. M. Benson, *Advances in Water Resources* **38** (2012) 48–59.
11. G. Daccord and R. Lenormand, *Nature* (1987) **325**, 41–43.
12. M. L. Hoefner and H. S. Fogler, *AIChE J.* (January 1988) **34**, 1, 45–54.
13. K. M. Hung, A. D. Hill and K. Sepehrnoori, SPE 16886, *J. Petroleum Technology* (1989) **41**, 1, 59–66.
14. M. A. Buijse, SPE 38166, 1997.
15. E. Bemer, O. Vincké and P. Longuemare, *Oil & Gas Science and Technology – Rev. IFP*, (2004) **59**, 4, 405–426.
16. P. Egermann, S. Bekri and O. Vizika, *Petrophysics* (2010) **51**, 1, 32–40.
17. E. Bemer and J. M. Lombard, *Oil & Gas Science and Technology – Rev. IFP* (2010) **65,** 3, 445–459.
18. K. E. Eide, Masters thesis, Norwegian University of Science and Technology, 2012.